Tailoring Properties of Metal-Free Catalysts for the Highly Efficient Desulfurization of Sour Gases under Harsh Conditions

Cuong Duong-Viet [1,2]**, Jean-Mario Nhut** [1]**, Tri Truong-Huu** [3]**, Giulia Tuci** [4]**, Lam Nguyen-Dinh** [3]**, Charlotte Pham** [5]**, Giuliano Giambastiani** [1,4,*]** and Cuong Pham-Huu** [1,*]

1 Institute of Chemistry and Processes for Energy, Environment and Health (ICPEES), UMR 7515 CNRS-University of Strasbourg (UdS), 25, rue Becquerel, CEDEX 02, 67087 Strasbourg, France; duongviet@unistra.fr (C.D.-V.); nhut@unistra.fr (J.-M.N.)
2 Ha-Noi University of Mining and Geology, 18 Pho Vien, Duc Thang, Bac Tu Liem, Ha-Noi 100000, Vietnam
3 Faculty of Chemical Engineering, The University of Da-Nang, University of Science and Technology, 54 Nguyen Luong Bang, Da-Nang 550000, Vietnam; thtri@dut.udn.vn (T.T.-H.); ndlam@dut.udn.vn (L.N.-D.)
4 Institute of Chemistry of OrganoMetallic Compounds, ICCOM-CNR Via Madonna del Piano, 10, Sesto F.no, 50019 Florence, Italy; giulia.tuci@iccom.cnr.it
5 SICAT SARL, 20 Place des Halles, 67000 Strasbourg, France; pham@sicatcatalyst.com
* Correspondence: giambastiani@unistra.fr (G.G.); cuong.pham-huu@unistra.fr (C.P.-H.)

Abstract: Carbon-based nanomaterials, particularly in the form of N-doped networks, are receiving the attention of the catalysis community as effective metal-free systems for a relatively wide range of industrially relevant transformations. Among them, they have drawn attention as highly valuable and durable catalysts for the selective hydrogen sulfide oxidation to elemental sulfur in the treatment of natural gas. In this contribution, we report the outstanding performance of N-C/SiC based composites obtained by the surface coating of a non-oxide ceramic with a mesoporous N-doped carbon phase, starting from commercially available and cheap food-grade components. Our study points out on the importance of controlling the chemical and morphological properties of the N-C phase to get more effective and robust catalysts suitable to operate H_2S removal from sour (acid) gases under severe desulfurization conditions (high GHSVs and concentrations of aromatics as sour gas stream contaminants). We firstly discuss the optimization of the SiC impregnation/thermal treatment sequences for the N-C phase growth as well as on the role of aromatic contaminants in concentrations as high as 4 vol.% on the catalyst performance and its stability on run. A long-term desulfurization process (up to 720 h), in the presence of intermittent toluene rates (as aromatic contaminant) and variable operative temperatures, has been used to validate the excellent performance of our optimized $N-C^2/SiC$ catalyst as well as to rationalize its unique stability and coke-resistance on run.

Keywords: mesoporous N-doped carbon coating; silicon carbide composites; gas-tail desulfurization treatment; BTX contaminants; elemental sulfur

1. Introduction

Natural gas (NG) is certainly the cleanest fossil fuel employed for energy purposes. At odds with other natural sources (i.e., petroleum and charcoal) [1], NG holds important environmental merits because it can produce more heat and light energy by mass while keeping its environmental impact significantly lower in terms of carbon footprint and other pollutants that contribute to smog and unhealthy air. The primary constituent of NG is methane (CH_4) but, depending on its origin, it may also contain higher hydrocarbons, including aromatics and sulfur-containing compounds, N_2, CO_2, He, H_2S and noble gases to various extents [2]. In this regard, a complex but effective sequence of thermal and catalytic transformations have been implemented for NG processing as to remove undesired compounds and preventing the diffusion of corrosive and potentially hazardous substances for human health and environment. In particular, organic and inorganic S-compounds removal from natural gas is a mandatory step before any gas manipulation/processing [3–5]. Indeed,

their presence besides being highly risky for the toxicity of selected species (e.g., H_2S) can led to undesired phenomena such as the fouling or even the permanent deactivation of catalysts employed in the gas processing. Although current catalytic technologies allow a selective and almost complete (up to 99.9%) hydrogen sulfide conversion into elemental sulfur [6], they still suffer from technical limitations linked to a progressive catalyst deactivation when desulfurization process is operated under harsh reaction conditions (gas hourly space velocity (GHSV) close to those employed in industrial plants), or in the presence of contaminants such as heavy hydrocarbons and aromatics (i.e., benzene, toluene and xylene (BTX)) [2] that are commonly present in untreated natural gas streams. Such impurities deeply impact the performance, stability, and lifetime of catalysts and detrimentally burden on the overall process economy balance. BTX (C $\geq$ 7) in particular can lead, throughout the desulfurization process, to the formation of carbonaceous or heavy carbon-sulfur deposits [7] whose incomplete removal translates into catalyst fouling phenomena with the subsequent alteration of its performance or—in worst cases—to the complete catalyst deactivation. Reduction of BTX concentration in acid gas streams is therefore a mandatory step before that gaseous streams reach the catalysts surface, thus increasing the process complexity as well as that of the reactor setup. Complementary and equally valuable technological options such as the use of either amine or solvent enrichment units (Acid Gas Enrichment units—AGE) [8] or the use of activated carbon beds [9] housed upstream of the catalytic desulfurization (SRU) unit, have successfully been implemented for BTX fractions removal.

Whatever the option at work, regeneration treatments of AGE or activated carbon units are periodically needed along with the downstream treatment of BTX wastes. These phases are costly and can cause the change of feed conditions in the desulfurization plant or even the complete feed shut down.

There are little doubts on the relevance of the selective H_2S oxidation to elemental sulfur from both an environmental and commercial viewpoint [10] (~75 Mt/year of elemental sulfur are globally produced from oil and gas processing units). However, the search for robust, highly effective and selective catalysts for the process remains a challenging area of research for the chemistry and engineering community engaged in the field. In particular, the development of robust and durable catalysts suitable to operate the selective H_2S oxidation under variable acid concentrations and showing an excellent resistance to aromatics deactivation is a highly challenging task and thus a widely investigated subject of research.

The last years have witnessed a growing interest of catalysis community towards the use of carbon nanomaterials as pure C-networks or light-heterodoped matrices (i.e., nanotubes (CNTs), nanofibers (CNFs) or thin-carbon film deposits, including N-doped counterparts) as metal-active phase supports or single-phase, metal-free catalysts for a wide series of chemical and electrochemical transformations [11,12]. Metal-free systems of this type have successfully been scrutinized as selective and efficient catalytic materials for a number of industrially relevant oxidation [13–18] and reduction [19–22] processes or as valuable promoters of other challenging catalytic transformations [23,24]. Nanocarbon-based materials, particularly in the form of N-doped networks, have already been exploited as effective metal-free systems for the selective hydrogen sulfide oxidation to elemental sulfur from natural gas tails [16,25–33]. The unique features of these single-phase systems (e.g., the absence of a metal active-phase, the prevalent basic surface character of the N-doped samples together with reduced production cost and environmental impact) have largely contributed to overcome the drawbacks classically encountered with metal nanoparticles-based catalysts. The absence of metal nanoparticles rules out unwanted sintering and leaching phenomena of the active phase occurring on heterogeneous catalysts typically operating under harsh reaction conditions. Moreover, their basic surface character can largely prevent the occurrence of cracking side-processes responsible for the rapid catalyst fouling with subsequent permanent alteration of its performance. This aspect is of particular relevance for catalytic materials operating in the presence of variable

concentrations of aromatics whose ultimate and detrimental effects are well known for metal-based catalysts of the state-of-the-art.

In recent years, our group has proposed a versatile technology for the coating of 3D-shaped materials (including open-cell foam structures with variable void fractions), with thin and highly N-enriched mesoporous carbon deposits [15,26,34]. Accordingly, selected 3D hosting matrices underwent successive soaking/impregnation cycles using an aqueous solution of cheap and food-grade components, followed by controlled drying/calcination/annealing steps. Such an approach to the N-C coating of macroscopically shaped networks, besides reducing the formation of toxic by-products typically encountered with more conventional Chemical-Vapor-Deposition (CVD)-based synthetic schemes, offers a versatile and straightforward tool to the easy upscale of challenging metal-free catalytic materials.

The combination of this coating technology with a non-oxide ceramic support (i.e., silicon carbide—SiC) has generated ideal catalyst candidates suitable to operate the selective H_2S desulfurization efficiently under relatively high acid gas concentrations and in the presence of high contents of aromatics as contaminants (0.5 vol.% $\leq$ (H_2S) $\leq$ 2 vol.%; 1000 ppm $\leq$ (tol) $\leq$ 20,000 ppm) [35,36]. SiC as a support for the N-C active phase was selected in light of its high chemical inertness and stability under acidic/oxidative or basic environments along with its excellent mechanical resistance that made it the ideal choice for the target process. Moreover, its medium thermal conductivity [37] prevents or reduces the generation of local temperature gradients (hot spots) while operating highly exothermic transformations [27,38,39]. This additional feature, not available with more classical oxide-based ceramics, contributes to the ultimate catalyst stability and its lifetime on stream.

This contribution takes advantage from our recent findings in the area of metal-free catalysts for the highly efficient and selective H_2S desulfurization and it aims at pointing out the importance of controlling the morphological and chemical properties of the N-C phase to make a step forward in the direction of catalytic materials featured by improved desulfurization performance and resistance towards deactivation/fouling phenomena. We have recently demonstrated the excellent performance of a N-C/SiC catalyst in the presence of relatively high concentrations of toluene (up to 20,000 ppm, 2 vol.%) as contaminant in a desulfurization process operated under relatively harsh reaction conditions (GHSV up to 2400 h^{-1}). We have also demonstrated the existence of a beneficial "solvent effect" played by toluene on the process selectivity as a distinctive feature of these metal-free catalytic materials. With these catalysts, the toluene present in the gas stream was found to facilitate the desorption and removal of elemental sulfur from the catalyst surface thus reducing the sulfur residence time in contact with the N-C network and preserving the process from the occurrence of undesired over-oxidation paths at the catalyst surface. Hereafter we demonstrate how a more appropriate control of the soaking/thermal treatment cycles in the N-C phase growth holds beneficial effects on the chemical and morphological properties of the latter as well as on the ultimate materials performance in the direct H_2S oxidation from sour gases [H_2S = 0.3 vol.%; O_2/H_2S = 2.5; GHSV up to 3200 h^{-1}) containing aromatic contaminants (i.e., toluene) at concentrations as high as 40,000 ppm (4 vol.%). It should be pointed out that such a toluene concentration is markedly higher compared to that traditionally encountered in sour gas stream (i.e., 1200–2100 ppm) and it has been deliberately employed to validate the remarkable resistance of our metal-free catalyst towards BTX deactivation phenomena. To address these goals a new impregnation/thermal sequence for the N-C phase growth on SiC extrudates is proposed and a comparison with that previously reported by us has been used to shed light on the ideal chemical and morphological properties of the N-C phase for the desulfurization process to occur. In addition, N-C/SiC performance has been compared with that of the benchmark Fe_2O_3/SiO_2 catalyst [40] for the sake of completeness.

2. Results and Discussion

2.1. Catalysts Characterization and Properties of N-C^2/SiC and N-C^4/SiC

The SiC coating with the N-C phase was accomplished following two alternative sequences of the solid support soaking in a standardized impregnation solution and successive thermal treatments (see Section 3 for details). Figure 1 provides a visual sketch of the operative sequences employed for the preparation of N-C^2/SiC and N-C^4/SiC composites, respectively. At odds with N-C^4/SiC, it can be inferred that preparation of N-C^2/SiC follows a simplified synthetic path that includes only two impregnation/drying steps (green cycles) before undergoing annealing treatment at 900 °C for 2 h under inert atmosphere (red cycle) without passing any intermediate calcination step (orange cycle in N-C^4/SiC sequence).
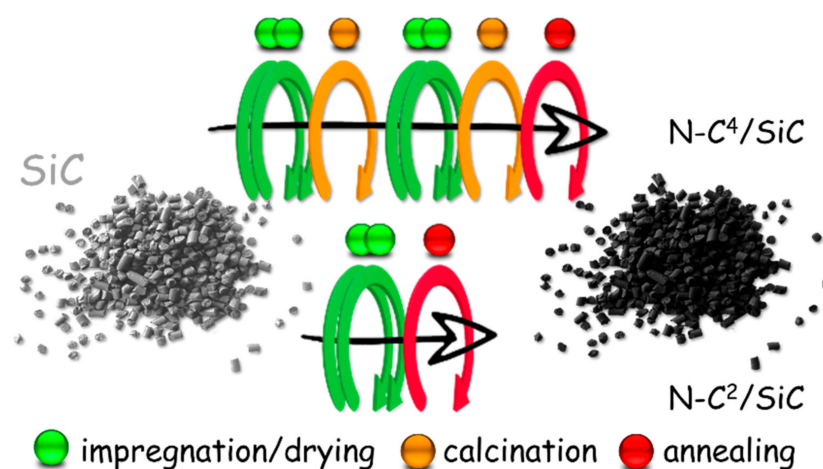
Figure 1. Quick visual representation of the two alternative synthetic paths used for the preparation of N-C^4/SiC (upper black arrow) and N-C^2/SiC (down black arrow) composites, respectively. Green cycles refer to the impregnation/drying steps, orange cycles refer to the material calcination at 400 °C for 2 h and red cycles refer to the material annealing at 900 °C for 2 h under Argon atmosphere.

Although a complete N-C^4/SiC characterization and its H$_2$S desulfurization properties have previously been detailed by us elsewhere, [26,34,36] their comparison with those of N-C^2/SiC is necessary to better highlight the improved properties and catalytic performance of the latter. Both composites (Figure 2A) were analyzed in terms of specific surface area (SSA), total pore volume and pore-size distribution by N$_2$ physisorption at the liquid N$_2$ temperature (77 K).

As Table 1 shows, the specific surface areas (SSA) of the two composites are very close each other and they are almost twice than that measured on the plain SiC support. Both composites present Type IV isothermal profiles (Figure 2A) with distinctive H$_2$ hysteresis loops in the 0.45–1.0 P/P$_0$ range, typical of mesoporous networks featured by complex pore structures of ill-defined shape [41]. Sample N-C^4/SiC presents a more pronounced hysteresis loop that is ascribed to the presence of a large extent of smaller mesopores and a lower mean pore-size distribution (Table 1) that facilitate the occurrence of capillary condensation phenomena. This datum is in line with the pore-volume distribution curves recorded on the three samples at comparison (Figure 2B). From the inspection of these profiles, it can be deduced a reduced content of small mesopores (in the 2–5 nm range) in N-C^2/SiC compared to its counterpart N-C^4/SiC, together with the presence of larger mesopores (prevalently in the 20-60 nm range) available on the former only. As far as N-C phase mass content is concerned, thermogravimetric analysis (TGA) on air (50 mL min^{-1}) on the two samples (Figure 2D) showed only negligible differences on the content of organic deposit (6.7 wt.% on N-C^2/SiC and 6.9 wt.% on N-C^4/SiC) whatever the catalyst preparation sequence adopted (Figure 1). Both profiles evidence a distinctive weight loss

at 622 and 613 °C for N-C^2/SiC and N-C^4/SiC, respectively, where the derivative of the thermogravimetric curves (DTG) holds its maximum value.
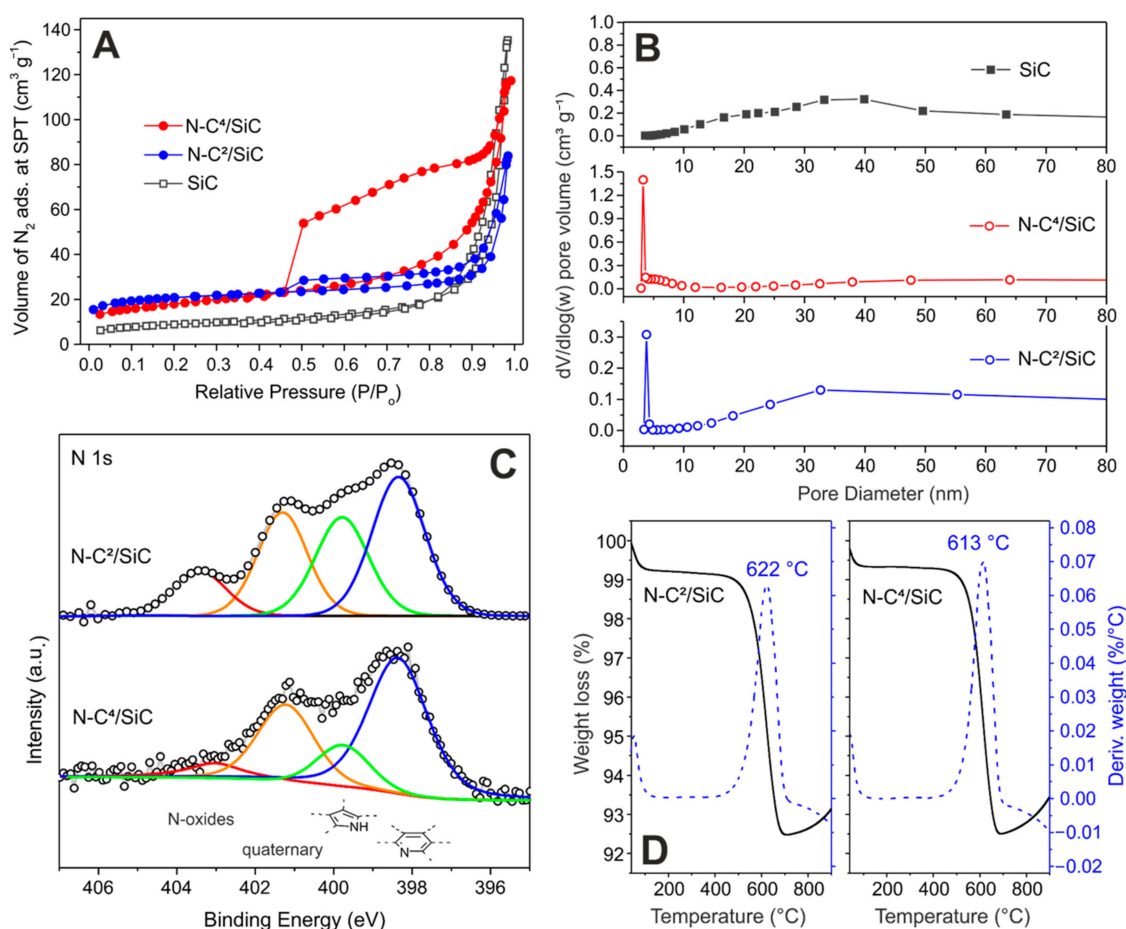
Figure 2. (**A**) N$_2$ adsorption-desorption isotherm linear plot of SiC (light grey curve), N-C^2/SiC (blue curve) and N-C^4/SiC samples (red curve) recorded at 77 K along with (**B**) the respective pore-size distributions measured (BJH method). (**C**) High-resolution XPS N 1s core level region of N-C^2/SiC (up) and N-C^4/SiC (down) at comparison, along with the relative curves fittings. (**D**) Thermogravimetric/derivative of the thermogravimetric curves (TG/DTG) profiles of N-C^2/SiC (left-side hand) and N-C^4/SiC (right-side hand) at comparison. Weight loss is measured arbitrarily in the 200–700 °C temperature range. Operative conditions: Air, 50 mL/min; heating rate: From 40 to 900 °C at 10 °C/min.

The XPS analysis of the materials at comparison confirmed the same composition providing largely superimposable survey profiles (Figure S3). The high-resolution N 1s analysis of the two samples has pointed out a slightly changed composition of the N-configurations available. Table 1 lists the relative % of the different N-species in the samples. N 1s peaks deconvolution (Figure 2C) accounts for three main components centered at 398.4 ± 0.2 eV (N-pyridinic—blue line), 399.7 ± 0.2 eV (N-pyrrolic—green line) and 401.2 ± 0.2 eV (N-quaternary—orange line), along with an additional shoulder (more pronounced in N-C^2/SiC) at higher binding energies (403.0 ± 0.3 eV—red line) and ascribed to the presence of N-oxidized species.

As Table 1 shows, the relative % of N-species obtained by the two alternative impregnation/thermal sequences (Figure 1) give rise to a redistribution of the N-configurations available at the materials surface. In particular, reducing the number of impregnation/drying steps and omitting the material calcination at 400 °C for 2 h, the percentage of pyrrole moieties is nearly doubled, that of N-oxide species increases, while that of basic N-pyridine sites decreases appreciably.

Table 1. Selected chemico-physical and morphological properties of catalysts and precursors.

Entry	Sample	SSA [a] (m^2 g^{-1})	Total Pore Volume (cm^3 g^{-1}) [b]	Average Pore Size (nm) [c]	Surface Basic Sites (mmol g^{-1}) [d]	N-C wt.% (from TGA)	N wt.% (from EA)	XPS Data, N-Species (%) [f]				
								N at.% [e]	Pyridinic	Pyrrolic	Graphitic	Oxidized
1	SiC	30	0.21	27.3	- [g]	-	-	-	-	-	-	-
2	N-C^2/SiC	69	0.11	14.8	0.63	6.7	2.1	5.1	36.8	26.0	25.6	11.6
3	N-C^4/SiC	61	0.18	5.6	0.45	6.9	1.5	4.5	53.1	13.1	26.8	7.0
4	Fe_2O_3/SiO_2	160	0.40	10.3	*n.d.*	-	-	-	-	-	-	-

[a] Brunauer-Emmett-Teller (BET) specific surface area (SSA) measured at T = 77 K. [b] Total pore volume determined using the adsorption branch of N_2 isotherm at $P/P_0 = 0.98$. [c] Determined by BJH desorption average pore width (4V/A). [d] measured by acid-base titration. [e] Determined by XPS analysis. [f] Determined by high resolution XPS N 1s core region and its relative peak deconvolution. [g] The pH value of an aqueous SiC dispersion lies close to pH 6.6 whereas the pH value of aqueous N-C^x/SiC dispersions (x = 2, 4) ranks close to 9.4. Data reported for elemental analysis (EA) and acid-base titration are calculated as the mean values over three independent runs. *n.d.* = not determined.

At odds with this trend, a quantitative estimation of basic sites available at the surface of both catalysts carried out by acid-base titration (see Section 3) has unveiled the higher basic character of N-C^2/SiC (0.63 mmol g^{-1}) respect to N-C^4/SiC (0.45 mmol g^{-1}). This discrepancy can be justified by the higher N-content of the N-C phase in N-C^2/SiC. Indeed, according to the N-C wt.% measured by TGA on the two samples (see Table 1 and Figure 2D) and the N wt.% measured by EA (Table 1), the N wt.% content normalized to the weight of N-C coating was calculated in 22 N wt.% and 31 N wt.% for N-C^4/SiC and N-C^2/SiC, respectively. In spite of a reduction in the percentage of basic pyridine sites for N-C^2/SiC, its markedly higher N-content reasonably accounts for its higher basic surface character [26,42].

2.2. Desulfurization Performance of N-C^2/SiC and N-C^4/SiC in the Presence of a Relatively High Vol.% of Toluene as Acid Gas Contaminant

The catalysts screening in the sour gas desulfurization starts from the awareness that aromatic contaminants like toluene hold a positive "solvent effect" on the catalytic outcomes of these metal-free systems [36]. Indeed, they favor a faster removal of sulfur deposits from the material mesopores, thus preventing the occurrence of undesired over-oxidation paths. In a recent desulfurization report with N-C^4/SiC, we have already shown the remarkably high resistance of this metal-free catalyst towards deactivation/fouling in the presence of toluene as the acid gas stream contaminant up to 5000 ppm. We also claimed an increase of the elemental sulfur rate up to 30% compared to selectivity values recorded for the same metal-free catalyst operated under identical—but toluene-free—conditions [36]. The comparative study between N-C^4/SiC and N-C^2/SiC points out on the importance of controlling the morphology and chemical composition of the N-C phase in order to get more robust, selective and efficient desulfurization catalysts suitable to operate the process under severe operative conditions. In this study, toluene was selected again as a model aromatic contaminant in sour gases [43] and the performance of two metal-free systems were compared for the sake of completeness with that of the benchmark Fe_2O_3/SiO_2 catalyst under the same conditions.

Aimed at stressing the relevance of morphological and chemical surface properties of N-C active phase in the process, we deliberately selected harsh operative conditions since the beginning of the desulfurization reaction. The process was then followed for a relatively long time (>200 h) and until the three samples clearly followed distinct catalytic paths. As a first trial, a mixture of H_2S (0.3 vol.%; O_2-to-H_2S ratio = 2.5; steam: 10 vol.%) and toluene (40,000 ppm; 4 vol.%) was passed downward the catalyst bed (6 g, V_{cat} ~7.5 cm^3 for N-C^4/SiC and N-C^2/SiC and 6 g, V_{cat} ~5.8 cm^3 for Fe_2O_3/SiO_2) heated at 210 °C and with a GHSV of 3200 h^{-1} (STP) (Figure 3A).
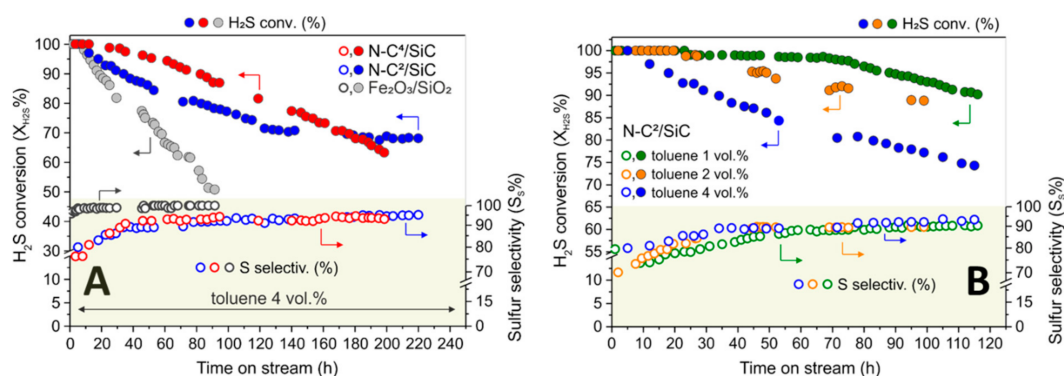
Figure 3. (**A**) Desulfurization performance on N-C^2/SiC, N-C^4/SiC and Fe$_2$O$_3$/SiO$_2$ catalysts of an acid gas stream ([H$_2$S] = 0.3 vol.%) in the presence of 40,000 ppm of toluene (4 vol.%) as contaminant in the stream. Catalysis details: 6 g (V$_{cat}$ ~ 7.5 cm^3 for N-C^4/SiC and N-C^2/SiC) or 6 g (V$_{cat}$ ~ 5.8 cm^3 for Fe$_2$O$_3$/SiO$_2$); O$_2$-to-H$_2$S ratio = 2.5, [H$_2$O] = 10 vol.%, He (balance); reaction temperature = 210 °C, GHSV (STP) = 3200 h^{-1}. (**B**) Desulfurization performance on N-C^2/SiC at variable toluene concentrations (10,000, 20,000 and 40,000 ppm or 1, 2 and 4 vol.%).

The long-term desulfurization process (up to 220 h) in the presence of 40,000 ppm of toluene in the stream served to highlight the excellent sulfur selectivity (S$_S$ up to ~94% with N-C^2/SiC at the steady-state-conditions) as well as the remarkably high coke resistance of both metal-free catalysts under severe and prolonged operative conditions. As Figure 3A shows, all catalysts ensure a quantitative H$_2$S conversion (100%) within the first 10 h on stream. Afterwards, H$_2$S conversion (X$_{H2S}$) decreases appreciably whatever the nature of the catalyst employed, with the benchmark Fe$_2$O$_3$/SiO$_2$ showing the much faster deactivation rate compared to its metal-free counterparts. Under these conditions, the iron-based catalyst shows a quantitative selectivity towards elemental sulfur although the high toluene content in the gas stream rapidly compromises its H$_2$S conversion capacity that falls below 50% just after 85 h on reaction. In spite of a slightly lower sulfur selectivity (S$_S$ in the 93–95% range), N-C^2/SiC and N-C^4/SiC show a markedly higher deactivation resistance and follow distinct deactivation paths. The N-C^4/SiC starts an appreciable deactivation only after 25 h on stream. Afterwards, X$_{H2S}$ gradually but constantly decreases down to 65% (after ~200 h on reaction). Noteworthily, N-C^2/SiC shows a more rapid deactivation in the first hours on stream that however reaches a H$_2$S conversion plateau around 160 h that is almost constantly maintained even after 220 h. As far as sulfur selectivity is concerned, both metal-free catalysts constantly rank above 90%. According to our previous report, the positive S$_S$ increase is ascribable to a co-solvent action played by toluene. Indeed, it facilitates the dissolution of sulfur deposits thus reducing their contact time with the N-C active phase and hence limiting the occurrence of undesired over-oxidation paths. The higher stability of N-C^2 active phase must be searched in the minor but critical chemical and morphological differences with N-C^4 phase and hence within the simplified impregnation/thermal sequence for the synthesis of N-C^2/SiC compared to N-C^4/SiC. It can be inferred that a larger mean pore size distribution in N-C^2 (Table 1, entry 2 vs. 3), a lower percentage of small mesopores in favor of larger ones (Figure 2B) together with a higher basic surface character of the sample (Table 1) account for its improved catalytic performance. Indeed, larger mesopores reduce the occurrence of pore clogging phenomena, ensure a more effective reagents access to the catalyst active phase and allow a more effective toluene scrubbing action towards the formed sulfur deposits. At the same time, a higher basic surface character creates the ideal microenvironment for the generation of local H$_2$S gradients and reduces the occurrence of cracking side-processes responsible for undesired "catalyst coking" [15,44–46]. The ability of N-C^2/SiC to stabilize on a relatively high H$_2$S conversion values is attributed to the simultaneous occurrence of all these phenomena. Selectivity values up to 94% at the steady-state conditions together with a X$_{H2S}$ constantly lying on 68% denote an efficient and selective desulfurization process where the toluene constant rate in the stream no longer affects the catalyst performance. On the other hand, it

positively influences the process selectivity and dynamically controls the accumulation of sulfur that might compromise the catalyst performance, particularly on long-term desulfurization runs. All of this evidence taken together underline the importance of controlling the chemical and morphological properties of the N-C phase through a rational optimization of the SiC impregnation/thermal treatment sequences thus allowing a tuning of the active phase surface properties as a function of its downstream application.

Expectedly, the lower the toluene content in the stream the slower the N-C^2/SiC deactivation rate under desulfurization conditions. This trend is confirmed by the catalyst deactivation measured with N-C^2/SiC in the presence of variable toluene concentrations (from 1 vol.% to 4 vol.%) within a 115 h desulfurization run (Figure 3B). At the same time, selectivity follows a similar and positive trend irrespective from the toluene content but reaching appreciably higher values when the concentration of the latter increases.

As an additional trial, N-C^2/SiC desulfurization capacity was investigated as a function of the reaction temperature and in the presence of variable percentages of toluene as contaminant. To this aim, N-C^2/SiC was initially conditioned at 210 °C using a toluene-free sour gas stream and the process was constantly monitored throughout about 50 h. During this time, the catalyst showed a quantitative H$_2$S conversion (X$_{H2S}$) and a sulfur selectivity (S$_S$ %) laying around 55–60% (Figure 4). The addition of toluene (4 vol.%) to the acid gas stream leads to the rapid increase of the process selectivity (up to 96%) while X$_{H2S}$ gradually stabilizes to a constant plateau value. An increase of the catalyst temperature to 230 °C results into a rapid X$_{H2S}$ increase that reaches values close to 80% for gradually dropping down to 72% after additional 100 h on stream.
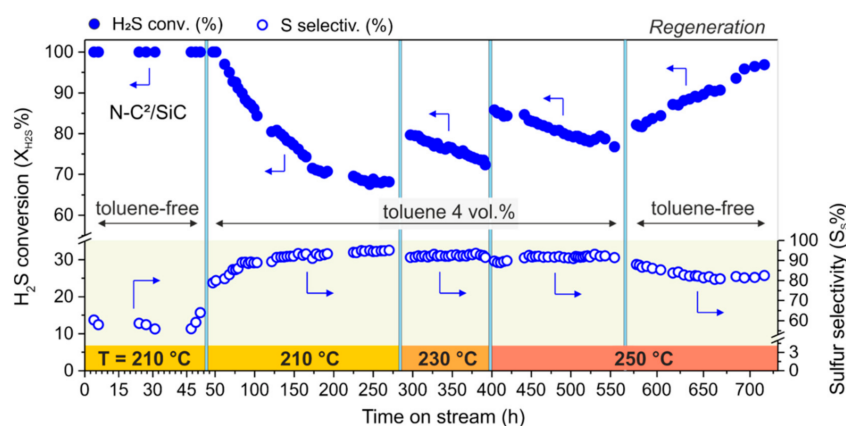
Figure 4. Effect of the temperature on the desulfurization performance of N-C^2/SiC using an acid gas stream ([H$_2$S] = 0.3 vol.%) in the presence of 40,000 ppm of toluene (4 vol.%) as contaminant. The first 47 h on stream were operated under toluene-free conditions. Catalysis details: 6 g (V$_{cat}$ ~ 7.5 cm^3 of N-C^2/SiC); O$_2$-to-H$_2$S ratio = 2.5, [H$_2$O] = 10 vol.%, He (balance); GHSV (STP) = 3200 h^{-1}. Catalyst regeneration (last 150 h on stream) occurs upon switching-off the toluene content from the acid gas stream.

As far as sulfur selectivity is concerned, the reaction temperature and X$_{H2S}$ increase affect only marginally its mean value that slightly reduces from 96% to 95%. Similarly, an additional temperature increase from 230 to 250 °C gives rise to a further increase of H$_2$S conversion values that grow over 85% while S$_S$ does no longer reduce appreciably. As Figure 4 shows, the X$_{H2S}$ decreases again and finally stabilizes around 78% after additional 120 h on stream together with a mean S$_S$ value of 93% that highlight the unique desulfurization properties of this metal-free catalyst while stressing again its robustness and durability under quite unconventional conditions. It should be noticed that N-C^2/SiC still maintains a remarkably high X$_{H2S}$ and S$_S$ even after more than a 3 weeks (550 h) H$_2$S desulfurization run operated under continuum mode and severe operative conditions.

Notably, switching-off toluene from the acid gas stream, translates into a gradual but complete recovery of the pristine catalyst performance (Figure 4, Regeneration section).

This positive trend in the absence of harsher oxidative conditions, led us to consider the action of toluene on the performance of our metal-free catalyst as that of an "interfering solvent" rather than a source of carbon for the growth of coke deposits. Indeed, the toluene confinement into the pores of the catalyst active phase alters the performance of the latter reversibly without causing any real catalyst coking and thus any irreversible deactivation. If the use of steam is known to be functional to the process by creating a thin water film on N-C surface that favors the diffusion of hydrophilic H_2S molecules into the catalyst pores, [28] the co-existence with a hydrophobic co-solvent (e.g., toluene) will translate into a depletion of reagents uptake and their diffusion towards the catalyst active sites. Anyhow, once toluene molecules are gradually desorbed from the pores and channels of the N-C network by using a toluene-free sour gas stream, the catalyst recovers its original performance.

The excellent coke resistance of N-C^2/SiC catalyst in the presence of relatively high concentrations of aromatics in the gas stream (40,000 ppm), has been confirmed by the analysis of the recovered N-C^2/SiC (spent catalyst) after 720 h on reaction. Figure 5A refers to the TGA analysis of the freshly prepared N-C^2/SiC (left-side hand) with its spent (right-side hand) counterpart put at comparison.
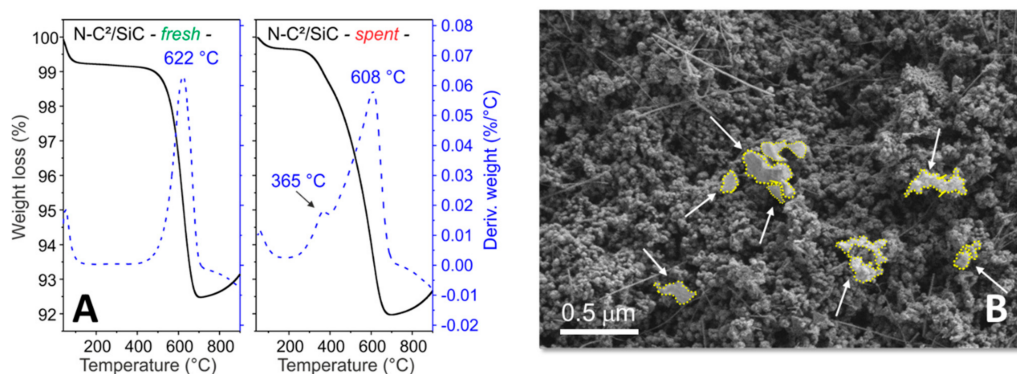
Figure 5. (**A**) TG/DTG profiles of the freshly prepared N-C^2/SiC (left-side hand) and its exhaust counterpart (right-side hand) at comparison. Weight loss is measured arbitrarily in the 200–700 °C temperature range and it corresponded to: 6.7 wt. loss % on the fresh N-C^2/SiC and 7.6 wt. loss % on the spent N-C^2/SiC. Operative conditions: Air, 50 mL/min; heating rate: from 40 to 900 °C at 10 °C/min. (**B**) SEM micrograph of N-C^2/SiC after its recovery at the end of a long-term catalytic run of 720 h. White arrows indicate residual sulfur deposits marked all around by yellow dashed lines.

The spent sample presents a minor shoulder featured by a maximum weight loss centered around 365 °C that accounts for about 0.9% of the overall weigh loss after the complete N-C active phase burning. Although we cannot definitively rule out the generation to a certain extent of low-melting coke deposits, we believe that such a little shoulder in the TGA profile of the exhaust sample is reasonably ascribable to the oxidation of sulfur residues. In spite of a temperature in the last part of the catalytic run (250 °C) that is higher than the sulfur dewpoint, some residues still remain available on the catalyst surface. Indeed, the SEM analysis of the recovered N-C^2/SiC (Figure 5B) clearly shows their presence in the form of patchy islands, whose generation is attributed to the residual catalyst activity during its cooling phase.

3. Experimental Section

3.1. Materials and Methods

β-SiC supports [extrudates (3 × 1 mm; $h \times \varnothing$), V = ~0.002 cm^3, SSA measured by N_2 physisorption (at 77 K) of 30 ± 1 m^2 g^{-1}] were provided by SICAT SARL (www.sicatcatalyst.com), thoroughly washed with deionized water in order to remove powdery fractions, hence dried at 130 °C overnight before use. Ammonium carbonate ((NH_4)$_2CO_3$, MW: 96.09 g mol^{-1}; Lot: A0356079), D-glucose 100% ($C_6H_{12}O_6$, MW: 180.16 g mol^{-1}) and citric acid ($C_6H_8O_7$ anhydrous, ≥99.5%, MW: 192.12 g mol^{-1}) were

provided by ACROS Organic[TM], MYPROTEINTM and VWR Chemicals, respectively. Unless otherwise stated, all reagents and solvents were used as provided by commercial suppliers without any further purification/treatment. N-C^4/SiC sample was prepared following the literature procedure previously reported by us [26,34,36] (and described in brief hereafter for the sake of completeness). N-C^2/SiC composite was prepared from the same soaking water solution of food-grade components, using a simplified impregnation/thermal sequence (vide infra). Scanning Electron Microscopy (SEM) was carried out on an UHR-SEM Gaia 3 FIB/SEM (TESCAN, Brno-Kohoutovice, Czech Republic). A 10 kV electron beam was used for SEM imaging operated in high-vacuum mode, using BSE and SE detectors. N$_2$ adsorption-desorption measurements were carried out on a Micromeritics® (Milan, Italy) sorptometer at the liquid N$_2$ temperature and relative pressures between 0.06 and 0.99 P/P$_0$. Each sample was outgassed at 250 °C under ultra-high vacuum for 8 h prior analysis in order to desorb moisture and adsorbed volatile species. The X-ray Photoelectron Spectroscopy (XPS) was carried out in an ultrahigh vacuum (UHV) spectrometer (Prevac, Rogów, Poland) equipped with a CLAM4 (MCD) hemispherical electron analyzer. The Al Kα line (1486.6 eV) of a dual anode X-ray source was used as incident radiation. Survey and high-resolution spectra were recorded in constant pass energy mode (100 and 20 eV, respectively). The CASA XPS program with a Gaussian-Lorentzian mix function and Shirley background subtraction was employed to deconvolute XPS spectra. Elemental analyses were performed on a Thermo FlashEA 1112 Series CHNS-O analyzer (Thermo Fisher Scientific, Waltham, MA, USA) and elemental average values were calculated over three independent runs. Powder Diffraction (PXRD) measurements were carried out on a Bruker D-8 Advance diffractometer (Bruker, Billerica, MA, USA) quipped with a Vantec detector (Cu Kα radiation) working at 40 kV and 40 mA. X-ray diffractogram was recorded in the 10–80° 2θ region at room temperature in air. Iron loading for the benchmark Fe$_2$O$_3$/SiO$_2$ was fixed by Inductively Coupled Plasma Atomic Emission spectrophotometry (ICP-AES) after sample acidic mineralization, using an Optima 2000 Perkin Elmer Inductively Coupled Plasma (ICP) Dual Vision instrument (Perkin Elmer Italia, Milan, Italy). Thermogravimetric analyses were performed on air (50 mL min^{-1}) from 40 to 900 °C (heating rate: 10 °C min^{-1}) on an EXSTAR Seiko 6200 analyser (Riga, Latvia). Acid-base titration was accomplished using the following procedure [47–49]: 10 mg of N-C^x/SiC (x = 2 or 4) were suspended in 7 mL of a standardized HCl solution (3 × 10^{-3} M, standardized with Na$_2$CO$_3$ as primary standard) and stirred at room temperature for 48 h. After that, three aliquots of the solution were titrated with a standardized NaOH solution (2.5 × 10^{-3} M). The basic sites loading was finally calculated as the average value over the three independent titration runs.

3.2. General Procedure for the Preparation of N-C^2/SiC and N-C^4/SiC Catalysts

N-C^2/SiC and N-C^4/SiC catalysts were prepared from the same water soaking solution for the SiC support but following different impregnation/thermal treatment sequences. The impregnation solution was prepared by dissolving at room temperature 3 g of D-glucose and 4.5 g of citric acid in 20 mL of ultrapure Milli-Q water. Afterwards, 3.46 g of ammonium carbonate were added to the stirred solution during which an effervescence due to CO$_2$ evolution starts (CAUTION! CO$_2$ effervescence needs to be carefully controlled during this phase by portioning the amount of (NH$_4$)$_2$CO$_3$ added over time). The as-prepared solution was used for the soaking/impregnation of 20 g of SiC extrudates whatever the nature of the target composite prepared (N-C^2/SiC or N-C^4/SiC) [34]. N-C^4/SiC was obtained following previously reported procedures [36]. Accordingly, SiC was soaked twice in the above water solution and excess of water—remaining after each impregnation step—was gently evaporated at 40 °C for 3 h. Afterwards, the solid was dried at 130 °C overnight before being calcined in air at 400 °C for 2 h (heating rate 2 °C min^{-1}). The as-obtained composite underwent identical impregnation/thermal treatment sequence at the end of which the sample was annealed at 900 °C (heating rate: 10 °C min^{-1}) for 2 h

under inert (Ar) atmosphere. As a result, a N-doped and mesoporous C-graphitic coat at the SiC outer surface was formed.

As far as N-C^2/SiC is concerned, it was obtained by soaking SiC twice in the impregnation solution, evaporating the excess of water at 40 °C for 2 h, drying the sample at 130 °C overnight before moving it directly to the annealing phase at 900 °C under inert atmosphere.

Fe$_2$O$_3$/SiO$_2$ (2.6 wt.% Fe) was prepared according to literature data [40]. To this aim, 10 g of SiO$_2$ powder were treated by incipient wetness impregnation with an aqueous solution of iron nitrate (Fe(NO$_3$)$_3$·9H$_2$O, 2.23 g; MW: 404,00 g mol^{-1}) in 10 mL of ultrapure Milli-Q water. The resulting solid was dried at 130 °C overnight before being calcined in air at 350 °C (heating rate: 5 °C min^{-1}) and maintained at the target temperature for additional 2 h before being used as such in catalysis. The final iron loading was measured by ICP-AES analysis and it was fixed to 2.6 wt.%. The XRD spectrum of the iron catalyst (Figure S1) was in accord with related literature reports [50].

Although the comparison of a metal-based catalyst with a metal-free one might appear as a meaningless exercise, Fe$_2$O$_3$/SiO$_2$ is a common benchmark system for the H$_2$S desulfurization, and its employment under conditions identical to those (hard) operated with the metal-free composites provides a clear-cut evidence of the superior performance and stability of the latter. Moreover, the direct H$_2$S oxidation to elemental sulfur in the presence of aromatics as contaminants in the gaseous stream is almost absent in the literature. In addition, SiO$_2$ as the metal active phase support was properly selected and compared with SiC, the latter being naturally coated by a thin layer of SiO$_x$C$_y$/SiO$_2$ once exposed to air at room temperature [27].

3.3. Selective H$_2$S Desulfurization of Sour Gases to Elemental Sulfur

The H$_2$S oxidation process can be described by Equations (1)–(3) reported below [51,52]. For catalytic trials, 6 g of N-C^2/SiC or N-C^4/SiC (V$_{cat}$ ~7.5 cm^3) were loaded on a silica wool pad, housed in a Pyrex tubular (∅$_{ID}$: 16 mm) reactor housed in a vertical electrical furnace, and the catalytic reactions were operated isothermally under atmospheric pressure. A graphical representation of the desulfurization scheme is provided on Figure S2.

$$2H_2S + O_2 \rightarrow 2S + 2H_2O \qquad \Delta H = -187 \text{ kJ/mol} \qquad (1)$$

$$S + O_2 \rightarrow SO_2 \qquad \Delta H = -297 \text{ kJ/mol} \qquad (2)$$

$$2H_2S + 3O_2 \rightarrow 2SO_2 + 2H_2O \qquad \Delta H = -518 \text{ kJ/mol} \qquad (3)$$
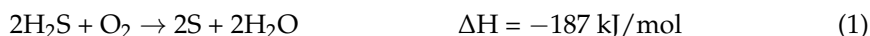
The temperature of the furnace was controlled by a K-type thermocouple and a Minicor regulator. The reactants gas mixture [H$_2$S (0.3 vol.%), O$_2$/H$_2$S = 2.5, H$_2$O (10 vol.%) in inert He as carrier (balance)] was passed downward through the catalyst bed, being gas flow rates monitored through Brooks 5850TR mass flow controllers. Steam (10 vol.%) was ensured by bubbling the inert carrier in a saturator containing hot water at 61 °C. CAUTION! *H$_2$S is a colourless, flammable, highly toxic gas. It must be handled—including its solutions—rigorously under a fume-hood and with all necessary precautions, especially a specific leak detector installed close to the operating setup.* The gas hourly space velocity (GHSV) was fixed at 3200 h^{-1} (corresponding to 400 mL min^{-1} or 4000 mL g$_{cat}$$^{-1}$ h^{-1}) and the O$_2$-to-H$_2$S molar ratio was kept constant to 2.5. The influence of toluene on the catalyst performance was investigated by feeding the reactants stream with toluene vapors at concentrations comprised between 1 vol.% (10,000 ppm) up to 4.0 vol.% (40,000 ppm). Toluene was fed-up in the stream by flowing He through a saturator containing pure toluene constantly maintained at 40 °C. To this purpose an independent line of He (Figure S2) was used to feed-up toluene in the reagents stream and its target concentration was adjusted by regulating the flow of the carrier. The amount of toluene passing through the catalyst was double checked by measuring the real liquid volume of toluene vaporized per day of experiment. All catalytic runs were carried out in continuous mode. Hence, most of the formed elemental sulfur was vaporized (because of the high partial pressure of sulfur

at the target reaction temperatures) and condensed alongside with steam at the reactor outlet in a trap maintained at room temperature. The analysis of the inlet and outlet gases was performed on-line using a Varian CP-3800 gas chromatograph (GC) equipped with a Chrompack CP SilicaPLOT capillary column and a thermal catharometer detector (TCD) for the detection of O_2, H_2S, H_2O, and SO_2 (down to 30 ppm). H_2S and SO_2 concentrations were recalculated on the basis of the corrected flow after steam condensation in a trap (Figure S2). All connecting lines were wrapped with thermal tapes maintained at 140 °C in order to prevent any condensation phenomena.

4. Conclusions

To summarize, the optimization of the SiC impregnation/thermal treatment sequences for the control of the surface chemistry and morphology of a highly N-rich carbon phase coating has been proposed. The new sequence for the N-C^2/SiC preparation has pointed out the importance of controlling the chemico-physical properties of the N-C phase as to get more efficient, selective and stable metal-free catalysts to be employed in the selective H_2S oxidation of sour gas streams and in the presence of aromatic contaminants concentrations as high as 40,000 ppm (4 vol.%). In the study, we have demonstrated how larger mesopores at the N-C active phase along with its higher basic surface character hold largely beneficial effects on the catalyst performance and its stability on stream. While the former reduces the occurrence of pore clogging phenomena, ensures a more effective reagents access to the catalyst active phase and allows a more effective scrubbing/removal action of the sulfur deposits by the toluene, the latter creates the ideal microenvironment for the generation of local H_2S gradients and reduces the occurrence of cracking side-processes responsible for the "catalyst coking". Most importantly, harsh H_2S desulfurization conditions in the presence of an intermittent toluene rate (from 0 to 4 vol.% and again down to 0 vol.%) in the sour gas stream has allowed to better elucidate the effect of aromatics on the performance and long-term stability of these metal-free desulfurization catalysts. Our results have pointed out that metal-free catalysts of this type suffer only marginally of irreversible deactivation caused by the generation of coke deposits. On the other hand, the reduced X_{H2S} efficiency in the presence of toluene can be reasonably ascribed to a competitive pore-filling by the toluene as the steam co-solvent. While steam facilitates H_2S diffusion into the pores and channels of the N-C active phase, the hydrophobic toluene can detrimentally compete with the reagent uptake on the catalyst active phase. However, once toluene molecules are gradually desorbed from the pores and channels of the N-C network (i.e., purging the catalyst under a toluene-free sour gas stream), the latter recovers its original performance.

Overall, three catalytic system at comparison (N-C^2/SiC, N-C^4/SiC and Fe_2O_3/SiO$_2$) have served to highlight the role of metal-free catalysts and their surface chemico-physical properties on their H_2S desulfurization performance in the presence of aromatics as contaminants. As shown in Figure 3A, while the iron-based catalyst rapidly deactivates because of the fouling of its active-phase (catalyst coking), the two metal-free systems behave differently as a function of their chemical and morphological properties. Under these conditions, the higher the basic surface properties and the higher the density of larger mesopores in the material, the higher the catalyst stability and durability on run.

Supplementary Materials: The following are available online at https://www.mdpi.com/2073-4344/11/2/226/s1, Figure S1: XRD profile of Fe_2O_3/SiO$_2$ catalyst (Fe 2.6 wt.%), Figure S2: Schematic representation of a desulfurization apparatus, Figure S3: XPS survey spectra of N-C^2/SiC and N-C^4/SiC.

Author Contributions: Conceptualization, C.P.-H. and G.G.; methodology, C.D.-V., C.P.H., J.-M.N., C.P. and G.G.; validation, C.D.-V., C.P.H., J.-M.N. and G.G.; formal analysis, C.D.-V., T.T.-H, G.T. and L.N.-D.; investigation, C.D.-V., C.P.H., J.-M.N., G.T. and G.G.; resources, C.P.-H., G.G., C.P. and L.N.-D.; data curation, C.D.-V., C.P.-H., G.T. and G.G.; writing—original draft preparation, G.G. and C.P.-H.; writing—review and editing, G.G., G.T., C.P., L.N.-D and C.P.-H.; supervision, C.P.-H., J.-M.N., G.G. and L.N.-D.; funding acquisition, C.P.-H., G.G. and L.N.-D. All authors have read and agreed to the published version of the manuscript.

Funding: This research was funded by the TRAINER project (Catalysts for Transition to Renewable Energy Future) of the "Make our Planet Great Again" program (Ref. ANR-17-MPGA-0017), the PRIN 2017 Project Multi-e (20179337R7) "Multielectron transfer for the conversion of small molecules: an enabling technology for the chemical use of renewable energy" and the Vietnam National Foundation for Science and Technology Development (NAFOSTED; grant number 104.05-2017.336). This research was also supported by SATT-Conectus through the DECORATE project.

Data Availability Statement: Data available on request.

Acknowledgments: SICAT SARL (www.sicatcatalyst.com) is gratefully acknowledged for providing SiC pellet samples.

Conflicts of Interest: The authors declare no conflict of interest.

References

1. Comparison Against Other Fossil Fuels. Available online: https://www.swarthmore.edu/environmental-studies-capstone/comparison-against-other-fossil-fuels (accessed on 7 December 2020).
2. Faramawy, S.; Zaki, T.; Sakr, A.A.-E. Natural gas origin, composition, and processing: A review. *J. Nat. Gas Sci. Eng.* **2016**, *34*, 34–54. [CrossRef]
3. Wieckowska, J. Catalytic and adsorptive desulphurization of gases. *Catal. Today* **1995**, *24*, 405–465. [CrossRef]
4. Eow, J.S. Recovery of Sulfur from Sour Acid Gas: A Review of the Technology. *Environ. Prog.* **2002**, *21*, 143–162. [CrossRef]
5. Piéplu, A.; Saur, O.; Lavalley, J.C.; Legendre, O.; Nédez, C. Claus Catalysis and H_2S Selective Oxidation. *Catal. Rev. Sci. Eng.* **1998**, *40*, 409–450. [CrossRef]
6. Zhang, X.; Tang, Y.; Qu, S.; Da, J.; Hao, Z. H_2S-Selective Catalytic Oxidation: Catalysts and Processes. *ACS Catal.* **2015**, *5*, 1053–1067. [CrossRef]
7. Ballaguet, J.-P.R.; Vaidya, M.M.; Duval, S.A.; Harale, A.; Khawajah, A.H.; Tammana, V.V.R. Sulfur Recovery Process for Treating Low to Medium Mole Percent Hydrogen Sulfide Gas Feeds with BTEX in a Claus Unit. U.S. Patent 9981848-B2, 29 May 2018.
8. Bahadori, A. *Natural Gas Processing Technology and Engineering Design*, 1st ed.; Gulf Professional Publishing: Houston, TX, USA, 2014.
9. Jahangiri, M.; Shahtaheri, S.J.; Adl, J.; Rashidi, A.; Kakooei, H.; Forushani, A.R.; Ganjali, M.R.; Ghorbanali, A. The adsorption of benzene, toluene and xylenes (BTX) on the carbon nanostructures: The study of different parameters. *Fresenius Environ. Bull.* **2011**, *20*, 1036–1045.
10. Sulphur Prices, Markets & Analysis. Available online: http://Www.Icis.Com/Fertilizers/Sulphur/ (accessed on 9 December 2020).
11. Serp, P.; Corrias, M.; Kalck, P. Carbon nanotubes and nanofibers in catalysis. *Appl. Catal. A Gen.* **2003**, *253*, 337–358. [CrossRef]
12. Su, D.S.; Perathoner, S.; Centi, G. Nanocarbons for the Development of Advanced Catalysts. *Chem. Rev.* **2013**, *113*, 5782–5816. [CrossRef]
13. Ba, H.; Luo, J.; Liu, Y.; Duong-Viet, C.; Tuci, G.; Giambastiani, G.; Nhut, J.-M.; Nguyen-Dinh, L.; Ersen, O.; Su, D.S.; et al. Macroscopically shaped monolith of nanodiamonds @nitrogen-enriched mesoporous carbon decorated SiC as a superiormetal-free catalyst for the styrene production. *Appl. Catal. B Environ.* **2017**, *200*, 343–350. [CrossRef]
14. Diao, J.; Feng, Z.; Huang, R.; Liu, H.; Hamid, S.B.A.; Su, D.S. Selective and Stable Ethylbenzene Dehydrogenation to Styrene over Nanodiamonds under Oxygen-lean Conditions. *ChemSusChem* **2016**, *9*, 662–669. [CrossRef]
15. Ba, H.; Liu, Y.; Truong-Phuoc, L.; Duong-Viet, C.; Nhut, J.-M.; Nguyen-Dinh, L.; Ersen, O.; Tuci, G.; Giambastiani, G.; Pham-Huu, C. N-Doped Food-Grade-Derived 3D Mesoporous Foams as Metal-Free Systems for Catalysis. *ACS Catal.* **2016**, *6*, 1408–1419. [CrossRef]
16. Chizari, K.; Deneuve, A.; Ersen, O.; Florea, I.; Liu, Y.; Edouard, D.; Janowska, I.; Begin, D.; Pham-Huu, C. Nitrogen-Doped Carbon Nanotubes as a Highly Active Metal-Free Catalyst for Selective Oxidation. *ChemSusChem* **2012**, *5*, 102–108. [CrossRef]
17. Li, M.; Xu, F.; Li, H.; Wang, Y. Nitrogen-doped porous carbon materials: Promising catalysts or catalyst supports for heterogeneous hydrogenation and oxidation. *Catal. Sci. Technol.* **2016**, *6*, 3670–3693. [CrossRef]
18. Luo, J.; Peng, F.; Wang, H.; Yu, H. Enhancing the catalytic activity of carbon nanotubes by nitrogen doping in the selective liquid phase oxidation of benzyl alcohol. *Catal. Commun.* **2013**, *39*, 44–49. [CrossRef]
19. Tang, C.; Zhang, Q. Nanocarbon for Oxygen Reduction Electrocatalysis: Dopants, Edges, and Defects. *Adv. Mater.* **2017**, *29*, 1604103. [CrossRef]
20. Zhang, L.; Jia, Y.; Yan, X.; Yao, X. Activity Origins in Nanocarbons for the Electrocatalytic Hydrogen Evolution Reaction. *Small* **2018**, *14*, e1800235. [CrossRef]
21. Zhao, S.; Wang, D.-W.; Amal, R.; Dai, L. Carbon-Based Metal-Free Catalysts for Key Reactions Involved in Energy Conversion and Storage. *Adv. Mater.* **2018**, *31*, e1801526. [CrossRef]
22. Tuci, G.; Filippi, J.; Ba, H.; Rossin, A.; Luconi, L.; Pham-Huu, C.; Vizza, F.; Giambastiani, G. How to Teach an Old Dog New (Electrochemical) Tricks: Aziridine-Functionalized CNTs as Efficient Electrocatalysts for the Selective CO_2 Reduction to CO. *J. Mater. Chem. A* **2018**, *6*, 16382–16389. [CrossRef]

23. Duan, X.; Ao, Z.; Sun, H.; Indrawirawan, S.; Wang, Y.; Kang, J.; Liang, F.; Zhu, Z.H.; Wang, S. Nitrogen-Doped Graphene for Generation and Evolution of Reactive Radicals by Metal-Free Catalysis. *ACS Appl. Mater. Interfaces* **2015**, *7*, 4169–4178. [CrossRef]

24. Yang, Y.; Zhang, W.; Ma, X.; Zhao, H.; Zhang, X. Facile Construction of Mesoporous N-Doped Carbons as Highly Efficient 4-Nitrophenol Reduction Catalysts. *ChemCatChem* **2015**, *7*, 3454–3459. [CrossRef]

25. Liu, Y.; Duong-Viet, C.; Luo, J.; Hébraud, A.; Schlatter, G.; Ersen, O.; Nhut, J.-N.; Pham-Huu, C. One-Pot Synthesis of a Nitrogen-Doped Carbon Composite by Electrospinning as a Metal-Free Catalyst for Oxidation of H_2S to Sulfur. *ChemCatChem* **2015**, *7*, 2957–2964. [CrossRef]

26. Ba, H.; Liu, Y.; Truong-Phuoc, L.; Duong-Viet, C.; Mu, X.; Doh, W.H.; Tran-Thanh, T.; Baaziz, W.; Nguyen-Dinh, L.; Nhut, J.-M.; et al. A highly N-doped carbon phase "dressing" of macroscopic supports for catalytic applications. *Chem. Commun.* **2015**, *51*, 14393–14396. [CrossRef]

27. Duong-Viet, C.; Ba, H.; El-Berrichi, Z.; Nhut, J.-M.; Ledoux, M.J.; Liu, Y.; Pham-Huu, C. Silicon carbide foam as a porous support platform for catalytic applications. *New J. Chem.* **2016**, *40*, 4285–4299. [CrossRef]

28. Sun, F.; Liu, J.; Chen, H.; Zhang, Z.; Qiao, W.; Long, D.; Ling, L. Nitrogen-Rich Mesoporous Carbons: Highly Efficient, Regenerable Metal-Free Catalysts for Low-Temperature Oxidation of H_2S. *ACS Catal.* **2013**, *3*, 862–870. [CrossRef]

29. Duong-Viet, C.; Truong-Phuoc, L.; Tran-Thanh, T.; Nhut, J.-M.; Nguyen-Dinh, L.; Janowska, I.; Begin, D.; Pham-Huu, C. Nitrogen-doped carbon nanotubes decorated silicon carbide as a metal-free catalyst for partial oxidation of H_2S. *Appl. Catal. A Gen.* **2014**, *482*, 397–406.

30. Ba, H.; Duong-Viet, C.; Liu, Y.; Nhut, J.-M.; Granger, P.; Ledoux, M.J.; Pham-Huu, C. Nitrogen-doped carbon nanotube spheres as metal-free catalysts for the partial oxidation of H_2S. *C. R. Chim.* **2016**, *19*, 1303–1309. [CrossRef]

31. Yu, Z.; Wang, X.; Hou, Y.-N.; Pan, X.; Zhao, Z.; Qiu, J. Nitrogen-doped mesoporous carbon nanosheets derived from metal-organic frameworks in a molten salt medium for efficient desulfurization. *Carbon* **2017**, *117*, 376–382. [CrossRef]

32. Shen, L.; Lei, G.; Fang, Y.; Cao, Y.; Wang, X.; Jiang, L. Polymeric carbon nitride nanomesh as an efficient and durable metal-free catalyst for oxidative desulfurization. *Chem. Commun.* **2018**, *54*, 2475–2478. [CrossRef]

33. Duong-Viet, C.; Ba, H.; Liu, Y.; Truong-Phuoc, L.; Nhut, J.M.; Pham-Huu, C. Nitrogen-doped carbon nanotubes on silicon carbide as a metal-free catalyst. *Chin. J. Catal.* **2014**, *35*, 906–913. [CrossRef]

34. Pham-Huu, C.; Giambastiani, G.; Liu, Y.; Ba, H.; Nguyen-Dinh, L.; Nhut, J.-M.; Duong-Viet, C. Method for preparing highly nitrogen-doped mesoporous carbon composites. EP Patent 3047905 A1, 29 April 2020.

35. Mokhatab, S.; Poe, W.A. (Eds.) Typical [H_2S] and [BTX] in sour gas are assumed close to 0.25 vol.% and about 2000 ppm, respectively, with the latter being tentatively composed by: Benzene = c.a. 900 ppm, Toluene = c.a. 750 ppm and Xylene = c.a. 400 ppm. In *Handbook of Natural Gas Transmission and Processing*; Gulf Professional Publishing: Houston, TX, USA, 2012.

36. Duong-Viet, C.; Nhut, J.-M.; Truong-Huu, T.; Tuci, G.; Nguyen-Dinh, L.; Liu, Y.; Pham, C.; Giambastiani, G.; Pham-Huu, C. A Nitrogen-Doped Carbon Coated Silicon Carbide as a Robust and Highly Efficient Metal-Free Catalyst for Sour Gases Desulfurization in the Presence of Aromatics as Contaminants. *Catal. Sci. Technol.* **2020**, *10*, 5487–5500. [CrossRef]

37. Mukasyan, A.S. Silicon Carbide. In *Concise Encyclopedia of Self-Propagating High-Temperature Synthesis*; Borovinskaya, I.P., Gromov, A.A., Levashov, E.A., Maksimov, Y.M., Mukasyan, A.S., Rogachev, A.S., Eds.; Elsevier Inc.: Amsterdam, The Netherlands, 2017; pp. 336–338.

38. Keller, N.; Pham-Huu, C.; Estournès, C.; Ledoux, M.J. Low temperature use of SiC-supported NiS_2-based catalysts for selective H_2S oxidation Role of SiC surface heterogeneity and nature of the active phase. *Appl. Catal. A Gen.* **2002**, *234*, 191–205. [CrossRef]

39. Nguyen, P.; Edouard, D.; Nhut, J.M.; Ledoux, M.J.; Pham, C.; Pham-Huu, C. High thermal conductive b-SiC for selective oxidation of H_2S: A new support for exothermal reactions. *Appl. Catal. B Environ.* **2007**, *76*, 300–310. [CrossRef]

40. Terörde, R.J.A.M.; van den Brink, P.J.; Visser, L.M.; van Dillen, A.J.; Geus, J.W. Selective oxidation of hydrogen sulfide to elemental sulfur using iron oxide catalysts on various supports. *Catal. Today* **1993**, *17*, 217–224. [CrossRef]

41. Sing, K.S.W.; Everett, D.H.; Haul, R.A.W.; Moscou, L.; Pierotti, R.A.; Rouquérol, J. Reporting Physisorption Data for Gas/Solid Systems with Special Reference to the Determination of Surface Area and Porosity. *Pure Appl. Chem.* **1985**, *57*, 603–619. [CrossRef]

42. Arrigo, R.; Hävecker, M.; Wrabetz, S.; Blume, R.; Lerch, M.; McGregor, J.; Parrott, E.P.J.; Zeitler, J.A.; Gladden, L.F.; Knop-Gericke, A.; et al. Tuning the Acid/Base Properties of Nanocarbons by Functionalization via Amination. *J. Am. Chem. Soc.* **2010**, *132*, 9616–9630. [CrossRef]

43. Toluene was also Selected on the Basis of Its Intermediate Toxicity Degree among BTX Contaminants, i.e., Xylene > Toluene > Benzene. Available online: http://universulphur.com/mespon/2015_presentations/session_b/5.%20Dealing%20with%20Aromatics%20in%20the%20Sulfur%20Recovery%20Unit%20--%20Eric%20Roisin%20--%20Axens.pdf (accessed on 21 December 2020).

44. Zhao, Z.; Dai, Y.; Ge, G.; Guo, X.; Wang, G. Facile simultaneous defect production and O,N-doping of carbon nanotubes with unexpected catalytic performance for clean and energy-saving production of styrene. *Green Chem.* **2015**, *17*, 3723–3727. [CrossRef]

45. Jin, X.; Balasubramanian, V.V.; Selvan, S.T.; Sawant, D.P.; Chari, M.A.; Lu, G.Q.; Vinu, A. Highly Ordered Mesoporous Carbon Nitride Nanoparticles with High Nitrogen Content: A Metal-Free Basic Catalyst. *Angew. Chem. Int. Ed.* **2009**, *48*, 7884–7887. [CrossRef]

46. Gounder, R.; Iglesia, E. Catalytic Consequences of Spatial Constraints and Acid Site Location for Monomolecular Alkane Activation on Zeolites. *J. Am. Chem. Soc.* **2009**, *131*, 1958–1971. [CrossRef]

47. Tuci, G.; Zafferoni, C.; Rossin, A.; Milella, A.; Luconi, L.; Innocenti, M.; Truong Phuoc, L.; Duong-Viet, C.; Pham-Huu, C.; Giambastiani, G. Chemically Functionalized Carbon Nanotubes with Pyridine Groups as Easily Tunable N-Decorated Nanomaterials for the Oxygen Reduction Reaction in Alkaline Medium. *Chem. Mater.* **2014**, *26*, 3460–3470. [CrossRef]

48. Tuci, G.; Luconi, L.; Rossin, A.; Berretti, E.; Ba, H.; Innocenti, M.; Yakhvarov, D.; Caporali, S.; Pham-Huu, C.; Giambastiani, G. Aziridine-Functionalized Multiwalled Carbon Nanotubes: Robust and Versatile Catalysts for the Oxygen Reduction Reaction and Knoevenagel Condensation. *ACS Appl. Mater. Interfaces* **2016**, *8*, 30099–30106. [CrossRef]

49. Moaseri, E.; Baniadam, M.; Maghrebi, M.; Karimi, M. A Simple Recoverable Titration Method for Quantitative Characterization of Amine-Functionalized Carbon Nanotubes. *Chem. Phys. Lett.* **2013**, *555*, 164–167. [CrossRef]

50. Cai, Z.; Leong, E.; Wang, Z.; Niu, W.; Zhang, W.; Ravaine, S.; Yakovlev, N.; Liu, Y.; Teng, J.; Lu, X. Sandwich-structured Fe_2O_3@SiO_2 @Au nanoparticles with magnetoplasmonic responses. *J. Mater. Chem. C.* **2015**, *3*, 11645–11652. [CrossRef]

51. Fahim, M.A.; Alsahhaf, T.A.; Elkilani, A. Fundamentals of Petroleum Refining. Elsevier, B.V.: Amsterdam, The Netherlands, 2010; pp. 377–402.

52. Ebbing, D.D.; Gammon, S.D. *General Chemistry*, 9th ed.; Houghton Mifflin Company: Boston, MA, USA, 2009.